A Study of *in situ* Reduction of MoO_3 to MoO_2 by X-ray Photoelectron Spectroscopy

Ben M. Garland,[1] Neal Fairley,[2] Nicholas C. Strandwitz,[1] Ryan Thorpe,[3] Pascal Bargiela[4] and Jonas Baltrusaitis[5,*]

[1]Materials Science and Engineering, Lehigh University, 5 E. Packer Ave., Bethlehem, PA 18015, USA

[2]Casa Software Ltd, Bay House, 5 Grosvenor Terrace, Teignmouth, Devon TQ14 8NE, UK

[3]Institute for Functional Materials and Devices, Lehigh University, 7 Asa Drive, Bethlehem, PA 18015, USA

[4]The Institute for Research on Catalysis and the Environment of Lyon (*IRCELYON)*, 2 Avenue Albert Einstein, 69626 Villeurbanne, France

[5]Department of Chemical and Biomolecular Engineering, Lehigh University, 111 Research Drive, Bethlehem, PA 18015, USA

Abstract

Results from X-ray Photoelectron Spectroscopy (XPS) of molybdenum oxide samples are presented to elucidate how Mo (VI) oxide evolves to Mo (IV) oxide upon heating of a MoO_3 sample. XPS data analysis techniques based on manipulation of spectra treated as vectors are shown and allow insights into intermediate phases of Mo oxide which suggest how the original oxide changes under the influence of heat but also supports an interpretation of as-received tetravalent Mo powders as multivalent materials. In particular, several new spectral components were observed and assigned to the Magnéli phase as well as MoO_3 domains that have been modified by the presence of X-rays or temperature. These assignments comprise a new method of data processing where sample modification is used to inform XPS data interpretation and differ from previous work where the linear relationship of the binding energy of molybdenum oxides has been used.

*Corresponding author: job314@lehigh.edu; +1-610-758 6836

Keywords: XPS; MoO_2; MoO_3; peak model; in situ

1. Introduction

Molybdenum oxides possess a diverse set of structural and electronic properties that warrant their use in research and commercial applications including catalysts, electronics, sensors, lubricants, superconductors, to name a few [1]. Molybdenum oxides are comprised of two binary oxide stoichiometries: Mo(VI) - MoO_3 and Mo(IV) - MoO_2. The corresponding polymorphs include the thermodynamically stable α-MoO_3, metastable β-MoO_3, ε-MoO_3 and hexagonal metastable h-MoO_3 [2]. The primary MoO_2 structure is that of distorted rutile [3]. The X-ray Photoelectron Spectroscopy (XPS) spectra of Mo (VI) oxides are relatively easy to obtain but relatively difficult to measure in a pure form. This is due to the fundamental problem where MoO_3 is affected by the X-rays during the measurements. In particular, exposing MoO_3 to X-rays induces chemical changes that can be observed in spectra [4,5]. This effect is largely due to the generation of substoichiometric phases of molybdenum oxides [6] and the high volatility of MoO_3 [7]. While the classical MoO_3 doublet pair of photoemission peaks can be observed in XPS, repeated measurements of Mo (VI) oxide demonstrate that under ambient temperature and UHV conditions, new shapes evolve at lower binding energy relative to the initial Mo 3d doublet [4,5]. Even when exposure to the measurement environment is limited, it is common to find the influence of X-ray and UHV exposure on observed Mo 3d spectra from Mo (VI) oxides. These changes to spectra are accelerated at higher temperatures and, once exposed to temperatures above a specific threshold, there is clear spectroscopic evidence that MoO_3 is converted to MoO_2 [8]. Spectral analysis of such thermally induced redox behavior has been of interest in early work where a linear relation between the binding energies and the oxidation numbers of the resulting molybdenum compound states was proposed [8]. This analysis resulted in XPS data Gaussian fits that yielded Mo(VI), Mo(V), Mo(IV) and Mo (II) with Mo (IV) two pairs of doublets due to isolated and paired double-bonded species at 230.4 eV. The assumption of the assignment of this second pair of Mo(IV) peaks was based on the fact that an additional doublet was needed to fully fit the spectral envelope. Similarly, Choi *et al*. performed MoO_3 reduction in H_2 at 673 K and a new state, $Mo^{\delta+}$, at 228.7 eV was observed and assigned to Mo^{3+} [9]. Spevack and McIntyre in their series of works on MoO_3 film reduction observed a series of peaks assigned to the main oxidation states of molybdenum [10]. An interesting observation was that thin films (~20 nm), upon reduction, yielded MoO_2 as the lowest oxidation state while bulk MoO_3 was reduced to metallic Mo [10]. The peak fitting procedure was based on well-defined molybdenum compounds spanning from Mo(VI) to Mo(IV) [11].

This linear spectral interpretation immediately found use in the catalysis community where this work [8,10,11] was highly cited but the validity of assignments was rarely scrutinized until Baltrusaitis and coworkers developed an informed amorphous sample model. In that model, lineshapes were created rather than isolated Gaussian peaks assigned to a specific oxidation state [4]. This approach was plausible due to the availability of multiple spectra acquired when exposed to X-rays with evolving structures. This approach provided for conceptually new XPS fit development procedures. In this manuscript, we further scrutinize the interpretation and assignments of molybdenum oxide spectra envelope with the focus on Mo (IV) assignments which, based on the previous work, are less certain due to data envelopes that contain multiple sets of doublet peaks. The question scrutinized in this work is to what extent the physical properties of Mo (IV) oxides generate these multiple doublet peaks or is the shape for Mo (IV) oxide Mo 3d data due to the persistence of Mo (VI) or Mo (V) oxides in materials predominantly Mo (IV) oxide. The answers to these questions are derived in this work through XPS data envelope monitoring of Mo (VI) oxide film deposited on Si substrate during heating from room to 723 K. These obtained data were then analysed by means of Principal Component Analysis (PCA), analysis of spectra by forming mathematically derived difference spectra, linear least squares fitting difference spectra to data and application of non-linear least squares fitting of synthetic curves to data.

2. Experiments and theoretical methods

2.1. MoO_3 thin film growth. Molybdenum oxide films were grown using thermal atomic layer deposition (ALD) [12][13] in an Ultratech-Cambridge Nanotech Savannah 100 system. Silicon (100) substrates were used. Before film growth, the substrates were treated with an isopropyl alcohol sonication, an 18.2 MΩ·cm H_2O rinse, a high purity N_2 dry, and 5 minutes of UV-ozone exposure with a Jelight Model 24. The substrates were held at 473 K and subject to sequential exposure to nitrogen-boosted $Mo(Nt\text{-}Bu)_2(NMe_2)_2$ pulses and an O_2/O_3 mixture with ~3 wt% of ozone under a continuous flow of N_2 carrier gas. The $Mo(Nt\text{-}Bu)_2(NMe_2)_2$ was held at 323 K. The deposition process consisted of 757 total ALD cycles, resulting in a Mo oxide film thickness of approximately 27 nm with a standard deviation among samples of 2.8 nm, as determined by J. A. Woollam variable angle spectroscopic ellipsometer (VASE) measurements. VASE was collected at 60° and 70° from 350 to 800 nm and fitted with an extended Cauchy model. Constant parameters were A = 1.812, B = 0.05039, C = 0.00048798, D = -0.00036982, IR = 0.41768, Urbach amplitude = 0.17926, and band edge = 4 eV.

2.2. XPS data acquisition

The XPS spectra of the thin MoO_3 films on Si upon thermal reduction were collected with a SPECS Near Atmospheric Pressure X-ray Photoelectron Spectroscopy (NAP- XPS) system. The NAP-XPS system is equipped with an XR 50 MF Al Kα X-ray Source with a μ-FOCUS 600 X-ray monochromator. The Al K_{α} radiation was used with an X-ray beam energy of 1486.7 eV and power of 120 W. A PHOIBOS NAP *in situ* 1D-DLD hemispherical electron energy analyzer (~0.85 eV energy resolution and 1 mm entrance aperture) collected the spectra. The sample holder was placed in a DeviSim NAP cell and heated using an e-beam from 300 to 873 K. The pressure during the entire NAP-XPS experiment was always kept at $\sim 10^{-8}$ mbar. Pass energy of 20 eV was utilized unless noted otherwise.

2.3. XPS data analysis methods

2.3.1. Methodological assumptions. Analysis of the spectral data was based on principles established for an informed amorphous model approach previously used to predict line shapes appropriate for Mo (VI) and Mo (IV) oxides [4]. Refinements to the method as described in this work make use of linear least squares and decomposition of data based on linear analysis to construct spectral shapes. The method described here differs since the precision in energy calibration becomes more important than using the method developed based on non-linear least squares and synthetic components [4]. Derivation of spectral shapes suitable for linear least squares and linear analysis requires the availability of spectra measured from a sample that evolves as a function of time and sample environment, aligned in energy during the continuous recording of the signal. This signal acquired during varying sample temperatures creates a series of spectra with characteristics amenable to linear analysis. This experiment thus is based on the expectation that sample potential is adequately maintained by electrical connection to the ground resulting in apparent binding energy scales that are consistent throughout all measurements of spectra, e.g. no charge calibration was performed. Assuming spectra are acquired under identical conditions resulting in spectra for which energy calibration used to align data channels with an energy reference is unnecessary, allowing measured spectra to be treated as vectors with coordinate values defined by intensity.

2.3.2. Spectral processing methodology. A least-squares criterion is defined for spectra constructed from histograms with n data bins $\boldsymbol{d} = \{d_1, d_2, d_3, \dots, d_n\}$ as follows. Given a set of linearly independent vectors in an n dimensional vector space $\{\boldsymbol{v_1}, \boldsymbol{v_2}, \boldsymbol{v_3}, \dots, \boldsymbol{v_m}\}$, a vector $\boldsymbol{y} = \{y_1, y_2, y_3, \dots, y_n\}$ can be defined by

$$\boldsymbol{y} = c_1\boldsymbol{v}_1 + c_2\boldsymbol{v_2} + c_3\boldsymbol{v_3} + \cdots + c_m\boldsymbol{v_m} \quad \dots \quad (1),$$

where $c_1, c_2, c_3, \dots, c_m$ are constant values. The vector $\boldsymbol{y}$ approximates $\boldsymbol{d}$. Each $\boldsymbol{v_j}$ is a spectral form representative of a chemical state.

The figure of merit used to select a set of constants $c_1, c_2, c_3, \dots, c_m$ that fit $\boldsymbol{y}$ to $\boldsymbol{d}$ is then

$$L(c_1, c_2, c_3, \dots, c_m) = \sum_{i=1}^{n}(y_i - d_i)^2 \quad \dots \quad (2).$$

The condition for minimizing the function $L(c_1, c_2, c_3, \dots, c_m)$ is

$$\frac{\partial L}{\partial c_j} = 0 \; for \; all \; j = 1,2,3, \dots, m \qquad (3).$$

If a matrix $\boldsymbol{A}$ is defined in terms of the vectors $\boldsymbol{v_j}$

$$\boldsymbol{A} = [\boldsymbol{v_1}, \boldsymbol{v_2}, \boldsymbol{v_3}, \dots, \boldsymbol{v_m}] \qquad (4),$$

then the set of simultaneous equations resulting from minimizing Equation (2) written in matrix notation becomes

$$\boldsymbol{A}^T\boldsymbol{A}\boldsymbol{c} = \boldsymbol{A}^T\boldsymbol{d} \qquad (5),$$

where $\boldsymbol{c} = \{c_1, c_2, c_3, \dots, c_m\}$. A least-squares problem has a theoretical solution, provided the inverse matrix $(\boldsymbol{A^T}\boldsymbol{A})^{-1}$ exists, in the form

$$\boldsymbol{c} = (\boldsymbol{A}^T\boldsymbol{A})^{-1}\boldsymbol{A}^T\boldsymbol{d} \quad \dots \qquad (6).$$

$\boldsymbol{A^T A}$ is a real symmetric matrix and therefore singular valued decomposition providing a least-squares solution even when $\boldsymbol{A^T A}$ is singular, hence an approximation $\boldsymbol{y}$ to $\boldsymbol{d}$ can always be obtained. However, not all solutions based on singular valued decomposition $\boldsymbol{y}$ are feasible solutions for spectra and therefore constraints forcing solutions with positive area must be introduced rather than simply a direct solution of Equation (6).

A solution based on Equation (6) is useful only if the vectors $\{\boldsymbol{v_1}, \boldsymbol{v_2}, \boldsymbol{v_3}, \dots, \boldsymbol{v_m}\}$ are spectroscopically and physically meaningful. It is assumed the number of vectors m is less than the number of spectra within the data set of interest. This assumption implies linear independence within the set of spectra is due to random noise and that fewer vectors with shapes that can be interpreted in terms of material properties allow a reduced set of vectors $\{\boldsymbol{v_1}, \boldsymbol{v_2}, \boldsymbol{v_3}, \dots, \boldsymbol{v_m}\}$ to be meaningfully applied to each spectrum $\boldsymbol{d}$ to obtain an approximation to spectra defined by Equation (1).

It is possible that a set of vectors$\{\boldsymbol{v_1}, \boldsymbol{v_2}, \boldsymbol{v_3}, \ldots, \boldsymbol{v_m}\}$ can be selected from within the original set of spectra. However, in the case of evolving spectra measured from Mo (VI) oxide, the evidence in Figure 1 suggests no set of spectra subsampled from experimental data is representative of intermediate reduced forms of Mo oxide necessary for an understanding of physical processes that evolve from Mo (VI) to Mo (IV). There is therefore a need to estimate spectral forms suitable for use in Equation (1) that are not available in the original data set. The method for constructing these more meaningful spectral shapes is to identify subsets of spectra for which a PCA indicates two abstract factors account for variation in the subset, then manipulate two spectra selected from the subset in an attempt to create spectral shapes open to physical interpretation. The creation of a suitable set of vectors $\{\boldsymbol{v_1}, \boldsymbol{v_2}, \boldsymbol{v_3}, \ldots, \boldsymbol{v_m}\}$ is achieved through trial and error, making use of prior knowledge and relationships within data to obtain a best-guess solution. While such an approach may seem a little lacking in rigor, it should be appreciated that these criteria are the same criteria used when constructing a peak model based on synthetic lines shapes and nonlinear optimization. The objective for analysis of a sample by both approaches is to obtain a superior understanding of the sample than is possible otherwise and there should be an awareness that a complete understanding is in general difficult to achieve for complex materials. All data processing was performed using CasaXPS processing software [14].

3. Results and Discussion

3.1. Evolution of spectral shapes of MoO_3 thin films with temperature

Figure 1 illustrates changes observed in Mo 3d spectra induced by temperature starting at 300 K, which was then raised to maintained at 723 K in 50-degree increments while high-resolution Mo 3d region spectra are measured continuously. The two peaks observed in Mo 3d region are due to the spin orbit coupling. Central to the analysis of these data is the stability of measurements in terms of binding energy and systematic errors caused by electronics and other instrumental factors. To validate these data as suitable for analysis based on vector methods, the set of spectra in Figure 1a was transformed into abstract spectra using PCA. The resulting abstract factors calculated from spectra in Figure 1a are shown in Figure 1b. PCA computed abstract factors from a set of spectra with an identical number of data channels resulting in a set of abstract factors representing an alternative basis set of vectors, which can be used to reproduce spectra through forming linear combinations of abstract factors. When summed with appropriate scaling, the computed abstract factors yield identical spectra to the original data set (within the round-off error associated with the PCA algorithm). The reason for performing a

PCA on these spectra is to examine abstract factors and identify a subset of abstract factors that can be used to reproduce raw spectra with precision consistent with random noise in data. On inspection of these abstract factors, it is clear there are three abstract factors (Figure 1b labeled 1, 2 and 3) that contain shapes necessary to describe as-recorded spectra. A fourth abstract factor (labeled 4) includes minor shapes, while the remaining abstract factors are mostly consistent with variations expected for random noise. These spectra were measured using pass energy 20 eV; therefore, sensitivity in collecting signals is relatively low and the dwell-time for each data channel is relatively long. As a consequence, there is the potential for systematic errors in these data, which result in minor shapes contributing to abstract factors with labels greater than 3. Nonetheless, there is sufficient evidence within these abstract factors to attempt a decomposition of spectra into three shapes that have characteristics of spectra. Three abstract factors result in reconstructed spectra that differ from raw spectra to a greater extent than expected for pulse-counted data. The residual standard deviation calculated from reconstructed spectra, making use of three abstract factors and raw spectra, is close to unity for fits that will be attempted based on spectral shapes of physical significance. Importantly, however, if four abstractors are used to reconstruct spectra, the residual standard deviation is closer to that expected for pulse counted spectra, so there is a suggestion four shapes are necessary to obtain good data reproduction for all spectra in the data set. Hence the set of vectors used to compute spectral shapes open to physical interpretation is calculated from the four most significant abstract factors labeled 1, 2, 3 and 4 in Figure 1b, but only three of these shapes may have interpretation in terms of oxidation state. The fourth shape is needed mathematically but may have some basis in sample evolution not easily identified with the chemical state.

3.2. Utilizing mathematical concepts to interpret temperature evolved XPS spectra of MoO_3 thin films

The steps used to convert spectra in Figure 1a to component spectra are described elsewhere [15,16]. The mathematical background to PCA and application of linear least squares to fitting spectra with component spectra are also described elsewhere [16]. Temperature-evolved MoO_3 thin film spectra interpreted as vectors are manipulated to form new spectral shapes that are open to physical interpretation. The two main mathematical steps leading to the ultimate solution are PCA and forming difference spectra. These mathematical steps are moderated by user choices that make use of prior knowledge about XPS features a temperature- or otherwise evolved MoO_3 [4]. In other words, the alternative to allowing *only* user intervention to guide solutions to avoid user bias is to prescribe statistical conditions which determine solutions similarly derived from these same mathematical steps. This latter approach is desirable because solutions are deemed systematic and are potentially open to using by researchers without the knowledge expected for a technique that applies mathematics in an informed way to XPS data.

3.2.1. The use of Principal Component Analysis and Vector Spaces

PCA abstract factors (AFs) are an output of a PCA calculation applied to a set of spectra shown in Figure 1a. The PCA calculation is facilitated by computing the eigenvectors of a covariance matrix formed from spectra. While the concepts underlying PCA can be defined using matrices, the relationship between the original spectra and PCA AFs is arguably best visualized graphically through the use of scatter plots. A scatter plot formed from two vectors allows a two-dimensional interpretation of how PCA relates to data, vectors and the dimension for a vector space. A scatter plot formed from two spectra is formed by plotting relative to some origin a set of points in a plane formed by x/y pairs gathered from each data bin in these two spectra where one spectrum supplies the set of x coordinates and the other spectrum supplies y coordinates. A scatter plot mathematically is making use of a concept from linear algebra, namely the rank of a matrix, where the matrix is formed from two spectra by arranging matrix elements with the intensity values for n data bins as follows in (7)

$$\begin{pmatrix} spectrum_1 \\ spectrum_2 \end{pmatrix} = \begin{pmatrix} d_{11} & d_{12} & \cdots & d_{1n} \\ d_{21} & d_{22} & \cdots & d_{2n} \end{pmatrix} \qquad (7).$$

According to linear algebra, the row rank for this matrix is equal to the column rank and since the column rank is at most two, plotting points formed from the columns of the matrix provides a graphical interpretation for the matrix concept of rank through plotting points in two-dimensions as shown in Figure 2. If two spectra are selected which are spectroscopically different as observed in thermally assisted MoO_3 thin film evolution in Figure 1a, then a scatter plot formed from these distinct spectra will have a distribution that extends over a two-dimensional plane. By contrast, if two spectra are chosen to be identical, then the set of points when plotted in a two-dimensional plane will appear plotted along a line drawn in that plane. These are illustrated in Figures 2 a and b, respectively. These characteristics of scatter plots are simple examples of data for which two nonzero abstract factors would be computed in the former case and only one nonzero abstract factor would be computed in the latter case. Further, if PCA is applied to two distinct spectra and a scatter plot is compiled from the resulting two AFs (labeled AF 1st and AF 2nd in Figure 2), then the essential shape for the scatter plot for the original spectra and the scatter plot for the AFs differ only in that the greatest variance in scattering points appears along the x-axis representing the principal AF. The act of performing a PCA analysis for two spectra shows that PCA offers a mathematical transformation for data that maintains the distribution of scatter points as the original data but provides a systematic way of calculating the spread of these scatter points. In the case of identical spectra, PCA clearly shows that two spectra transform into one dimension along the x-axis. In higher dimensions, PCA similarly transforms scatter plots (less available to graphical interpretation) and similarly provides AFs which are ordered by significance to shapes in original spectra. If PCA is applied to a set of vectors in higher dimensions where these vectors are almost identical, then PCA computes one nonzero AF and, for the other vectors in the set, a set of AFs that are effectively zero. Thus, applying the logic of PCA to sets of spectra allows the dimensionality for sets of spectra to be determined and in the context of working with the difference spectra, sets of spectra can be classified into subsets for which the dimension is close to two. Therefore, subsets of vectors can be identified that are open to a systematic analysis of shapes based on forming the difference spectra using two spectra selected from within these subsets.

3.2.2. Classification of Spectra by PCA and Difference Spectra

As explained in section 3.2.1, the set of Mo 3d spectra in Figure 1a can be classified by PCA into two subsets of spectra, each of which represents data that lie, in the absence of noise and minor systematic perturbations, within two planes, one plane per subset. The entire set of spectra PCA AFs, as illustrated in Figure 1b, appears to lie within a three-dimensional subspace, therefore these two planes when calculated should also lie within the same three-dimensional subspace. However, calculating four new spectral shapes from these two subsets yields four vectors with shapes that when PCA is applied to these four spectra, four AFs with significant shape result. This suggests that PCA applied to all spectra, as shown in Figure 1a, creates AFs that are orientated such that some proportion of significant spectral shape contributes to AFs of lesser importance, but without suggesting systematic signal within these lesser AFs. The conclusion from this observation is that a PCA applied to the full set of spectra in Figure 1a underestimates the number of dimensions in these data. It is therefore plausible to look for and make use of four spectral forms when fitting data in Figure 1a.

An explanation for the limitations of PCA applied to the entire set of spectra in Figure 1a lies at the heart of any PCA calculation. The first PCA AF shown in Figure 1b is similar to the mean average spectrum, but not in general identical to the mean average spectrum.

Nevertheless, if the mean average spectrum is representative of a significant proportion of spectra in the data set, then the lesser abstract factors represent deviations from this spectral shape and plotting the relative contributions of PCA AFs to fitting spectra reveal trends that appear to make sense as spectra move between two or more states of a material. However, if the average spectrum is distorted by some bias in how data are acquired, to accommodate the initial bias PCA AFs, which must be orthogonal to one another are forced to shapes that are not as sympathetic to the physical properties of spectra and to maintain the orthogonality of these PCA AFs mixing of information yields PCA AFs with noise characteristics which also include systematic information. Subsampling data sets to identify two-dimensional subsets tends to improve how representative these subsets is the first PCA AF. Hence the mixing of systematic trends and noise is less of a problem than if the full data set is used in a PCA calculation. The data set in Figure 1a is an example of where two trends can be identified and understood from a physical perspective. Phase changes in Mo oxide occur at different temperatures, with the consequence that two very different spectral shapes are present at the beginning and the end of the experiment. The bias in the PCA calculation is introduced by the length of time data are measured at these different temperatures and by implication the number of spectra available at each state. Hence the average spectrum is representative of neither set of spectra at these two different temperatures, with the side effect of pushing systematic information down the list of PCA AFs. Thus, classifying spectra using searching for spectra that lie in planes helps to understand the data as a whole.

Mo 3d spectra in Figure 1a are divided into two subsets of spectra as shown in Figure 3a. The initial four spectra are classified by PCA as different from the final six spectra. Dividing spectra into these two subsets and applying PCA separately to these two subsets results in each case in two AFs of significance for each subset of spectra (Figure 3b). Hence the assertion that two planes in a vector space can be identified by PCA. The results for PCA AFs shown in Figure 1b indicate three significant PCA AFs are determined when all spectra are included in the calculation. Thus, it is anticipated these two planes determined from these two subsets must include vectors that define the same three-dimensional subspace as the PCA AFs in Figure 1b. The challenge is to compute vectors from spectra in these two subsets that have plausible physical meaning and are capable of reconstructing each spectrum in Figure 1a with a similar figure of merit. PCA AFs are forced to be orthogonal vectors and by definition abstract mathematical entities, not generally open to physical interpretation. To achieve physical meaning for vectors there is a requirement to search for oblique linearly independent vectors.

Searching for physically meaningful vectors is achieved by forming from two spectra per subset, as classified by PCA into planes, sets of the difference spectra. Figure 4 presents an example of difference spectra formed from two spectra selected from subset 2 in Figure 3a. One of these difference spectra may be selected and used to assess the suitability of the selection in a mathematical sense by using the selected spectrum in a linear-least-squares fit to spectra in subset 2 and ultimately a fit to spectra in the entire set of spectra in Figure 1a illustrated in Figure 5. Physical justification for the selection requires prior knowledge about sample properties and an understanding of possible spectral shapes generated by photoemission.

Figure 4 shows a range of plausible difference spectra that might be interpreted as Mo (IV). This serves to demonstrate that a solution achieved by these means is not unique and therefore selecting a difference-spectrum based on mathematical grounds alone is unlikely to make the best possible choice. Likewise making an informed decision when choosing a difference-spectrum does not guarantee the solution is correct. It is therefore important to experiment with different choices and combinations of difference-spectra to investigate the consequences of different combinations to results similar to Figure 6, where trends are plotted that must also be open to physical interpretation. While this ambiguity may seem a disadvantage, the same ambiguity is present when peak models based on bell-shaped curves are used to analyze data such as these Mo 3d spectra. The advantage of calculating spectral shapes directly from data is that these shapes are constrained in shape by the data for which an analysis is required. By contrast, peak models based on synthetic line shapes have no such constraints, unless one deems mathematically defined bell-shaped curves to be the precise form for all photoemission from a given chemical state. The physics of metal oxides is seldom so simple as to yield a well-formed bell-shaped photoemission signal.

3.3. Resulting spectral shapes of thermally-evolved MoO_3 thin films

The application of these processing steps described in 3.2, however, relies on observations based on the initial data and is unique to any given analysis. Prior knowledge of spectral forms observed for standard molybdenum oxide measured by XPS is essential. For example, observing the spectrum for Mo 3d at 300 K close to shapes expected for Mo (VI) [4,10,17] is instrumental, as well as the awareness that Mo (VI), when measured under typical conditions for XPS, evolves in shape to some degree [4]. It is also helpful to know that Mo (IV) is an oxide with metallic characteristics [18] and manifests with Mo 3d line shapes that include bell-shaped structures with binding energy lower than the main Mo (VI) peaks. These Mo 3d line shapes and other line shapes compatible with the data set in Figure 1a are displayed scaled by linear least squares (LLS) fitting in proportions necessary to fit spectra in Figure 5.

Mo (VI) oxide formed as a thin film is expected to have a crystalline nanostructure. Hence, the initial spectrum measured at room temperature is a well-formed pair of bell-shaped doublet envelopes typical of a material in which valence electrons are localized. In bulk Mo (VI) oxide, the bandgap would typically require charge compensation for XPS photoemission. However, our results suggest the as-prepared sample is a film sufficiently thin to permit charge compensation from substrate photoemission and a stable steady-state potential during photoemission from Mo (VI) oxide. The results presented in Figure 5 assume this empirical observation is true. Once the sample is heated, the expectation is the conductivity of these samples increases with temperature. Further, reduced states of Mo oxide are suitable for measurement by maintaining the sample connected to the ground. Therefore, the primary source for uncertainty in peak positions is within the initial measurement before sample heating is performed.

The analysis leading to the results in Figure 5 also assumes the lowest oxidation state available while heating the Mo oxide is Mo (IV), in agreement with literature for thin molybdenum oxide films [10]. Two additional spectral components were required to allow for the intermediate state that develops, then recedes as the sample, as measured by XPS, is reduced from Mo (VI) oxide to a state mostly comprised of Mo (IV). The component spectrum in Figure 5 labeled Phase 1 is observed at temperatures at or below 673 K but is shown in Figure 5 to be present throughout the measurements for which Mo (IV) grows. Phase 1 forms immediately with the temperature application, and previously has been observed in the presence of X-rays [4]. As discussed later, we believe this phase represents Mo (VI), albeit with altered electronic structure, likely via defect formation due to X-rays. The fourth component shape that is evident at 723 K is more difficult to assign an oxidation state. This fourth phase is labeled *Magnéli Phase* to suggest a series of the varying stoichiometry oxidation state of Mo [19] which increases and decreases in population as better-defined higher oxidation states move to a lower oxidation state. This result, derived via systematic sample reduction with temperature and processed with the algorithms described in the *Spectral processing methodology* section, is very different from the previous interpretations of complex molybdenum oxide envelopes based on available standard model compounds since it allows to observe and quantify, for the first time, non-stoichiometric molybdenum oxide phase evolution.

The four-component curves used to fit data in Figure 5 represent one of many possible solutions to fitting these data using other shapes, all of which provide mathematical solutions. The solution selected for use in Figure 5 is deemed the most plausible solution based on factors that include two shapes. Phase 1 and Mo (VI) play a role in fitting data corresponding to temperatures at or below 673 K as well as 723 K. However, shapes labeled Magnéli phases and Mo (IV) only appear significantly within data collected with a sample temperature of 723 K, as shown in Figure 5. The fits shown in Figure 5, therefore, illustrate how heating Mo (VI) below some critical phase evolution temperature alters the initial material and these altered forms of Mo oxide are present and instrumental in the formation of Mo (IV) as the sample temperature is raised above the threshold temperature necessary for creating Mo (IV). Figure 6, which plots the percent area for these four Mo-oxide phases, suggests heating alone would find difficulty in fully reducing Mo (VI) to Mo (IV).

A comparison between the approach derived in this work leading to the results in Figure 5 and conventional modeling by fitting mathematical bell-shaped lines to data (Figure 7) demonstrates a similar result to that obtained in Figure 5d, except for the absence of the Magnéli phase in the conventional case. The construction of the peak model in Figure 7 is based on the component spectral shapes determined by the temperature-induced sample modification informed model. These line shapes in Figure 7 include asymmetry expected for Mo(IV) signal [18], which are modeled using a modified Doniach-Sunjic line shape [20] and include constrained sets of symmetric line shapes [21] component peaks that simulate signal corresponding to both Phase 1 and Mo(IV) curves in Figure 5d. Phase 1 here represents a combination of Mo (VI) and reduced species that form during the initial, low-temperature heating stage. Specifically, component spectra in Figure 5 derived from temperature evolved data suggest a sequence of substoichiometric phases of molybdenum and oxygen, labeled Magnéli phases. However, the conventional peak model in Figure 7 does not include the possibility of a substoichiometric signal but rather fits spectra with well-defined line shapes due to the changes in the peak area upon the fit. As a result, the complexity corresponding to Magnéli phases in Figure 5 is absent from the peak model in Figure 7. Nonetheless, both temperature-informed lineshapes (Figure 5) and the fitting of synthetic line shapes to data (shown in Figure 7) suggest the final state of the sample is a multivalent material, albeit leading to different speciation.

4. Conclusions

Spectra with multiple sets of doublet peaks associated with a given oxidation state are not uncommon in XPS. For example, tetravalent cerium oxide Ce 3d spectra are an example of photoemission data for which a given oxidation state is associated with multiple doublet peaks spread over many electron volts [22]. In this work, through the analysis of Mo 3d spectra, it has been shown that Mo (VI) reduces systematically to Mo (IV). Component spectra were computed that when fitted to raw spectra demonstrate systematic changes could be identified and quantified. Reduction induced by heating the sample above a threshold temperature can be understood in terms of spectral shapes (rather than synthetic components) which demonstrate that, when reduction is achieved by heating Mo oxide under vacuum, reduction to Mo (IV) is very slow. The analysis, as described in this paper, shows that Mo (VI), when heated, creates a spectral shape that significantly differs from the original Mo (VI) doublet measured at room temperature and demonstrates that XPS of Mo (VI) requires a careful assessment before attempting to interpret Mo 3d using a purely peak-model-approach based on synthetic line shapes. The results of these spectral shapes suggest that several phases are present in addition to peaks conventionally assigned to Mo (VI) and Mo (IV), such as Phase 1 identified here to possess the properties of Mo (VI) in the presence of temperature or X-ray induced defects, as well as substoichiometric Magnéli phases. The results fitted with synthetic bell-shaped components based on the informed lineshapes derived in this work show a cautionary tale where the fitting procedure itself modifies the number of physically meaningful components present by omitting the need to have Magnéli phases present, while still obtaining a mathematically reliable fit. The results presented here suggest that the molybdenum oxide data interpretation method based on the informed lineshapes provides much more physically meaningful information than a purely synthetic bell-shaped component fit, albeit both are mathematically feasible.

5. Acknowledgments

This work by J.B. was supported as part of UNCAGE-ME, an Energy Frontier Research Center funded by the U.S. Department of Energy, Office of Science, Basic Energy Sciences under Award No. DE-SC0012577. The CNRS is acknowledged for financial support to the Thematic Workshop (N° 1317144) held at the Station Biologique, Roscoff, France.

6. Author contributions

Ben M. Garland: Investigation (lead); Writing – review and editing (equal). Neal Fairley: Investigation (supporting); Methodology (lead); Writing – original draft (equal); Writing –

review and editing (equal). Nicholas C. Strandwitz: Writing – review and editing (equal). Ryan Thorpe: Investigation (supporting); Writing – review and editing (equal). Pascal Bargiela: Investigation (supporting); Writing – review and editing (equal). Jonas Baltrusaitis: Conceptualization (lead); Investigation (lead); Methodology (supporting); Supervision (lead); Writing – original draft (equal); Writing – review and editing (equal).

7. Competing interests.

The authors declare no competing interests.

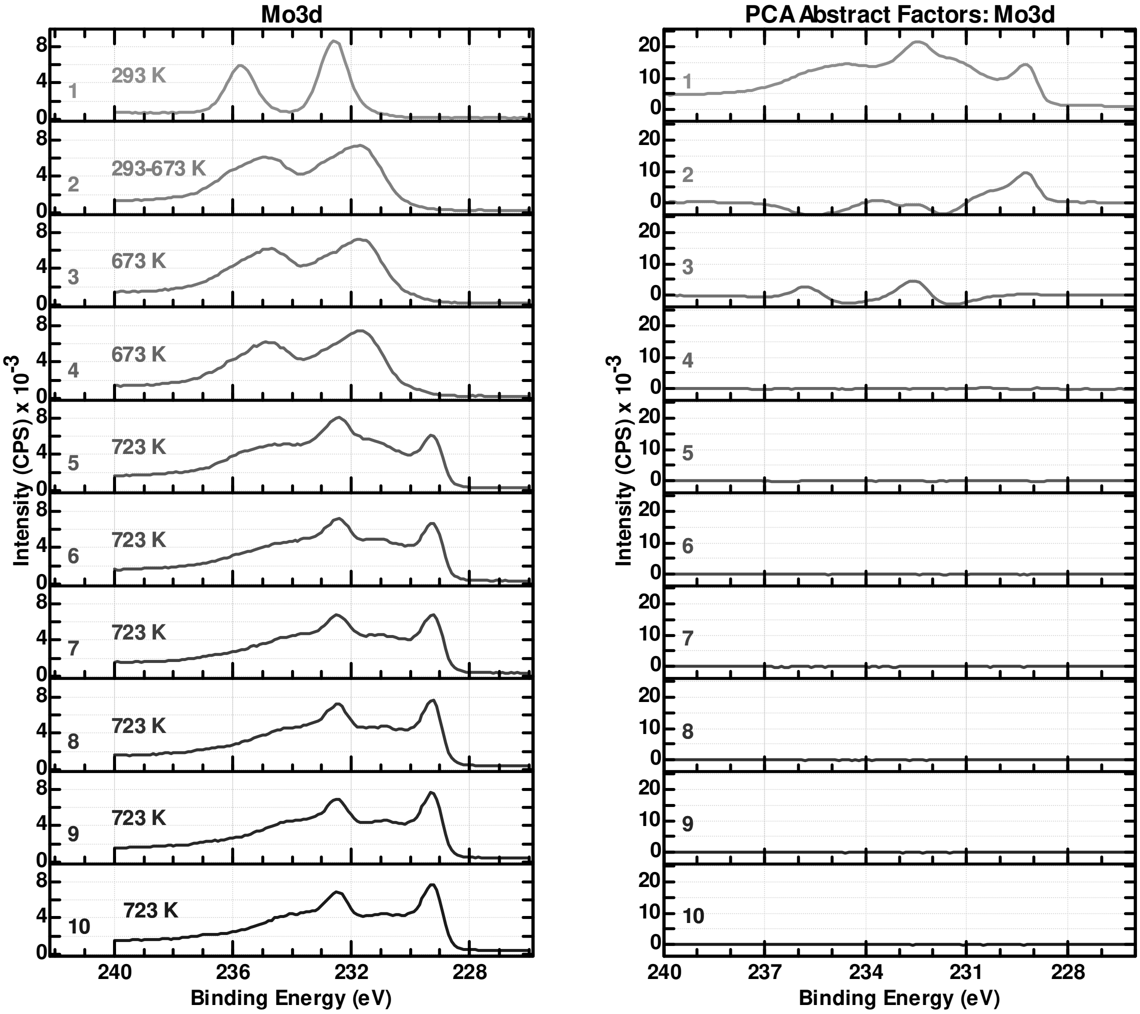

(a) (b)

Figure 1. (a) Mo 3d spectra measured from Mo (VI) oxide after exposure to temperatures indicated on the plot. Also indicated is the measurement index which represents a temporal influence on these data for a given temperature. (b) PCA abstract factors are calculated from spectra displayed in (a). The index assigned to each abstract factor is ordered according to the importance of abstract factors to photoemission signal for data in (a). The temperature labelled in Figure 1a was held at least 20 minutes.

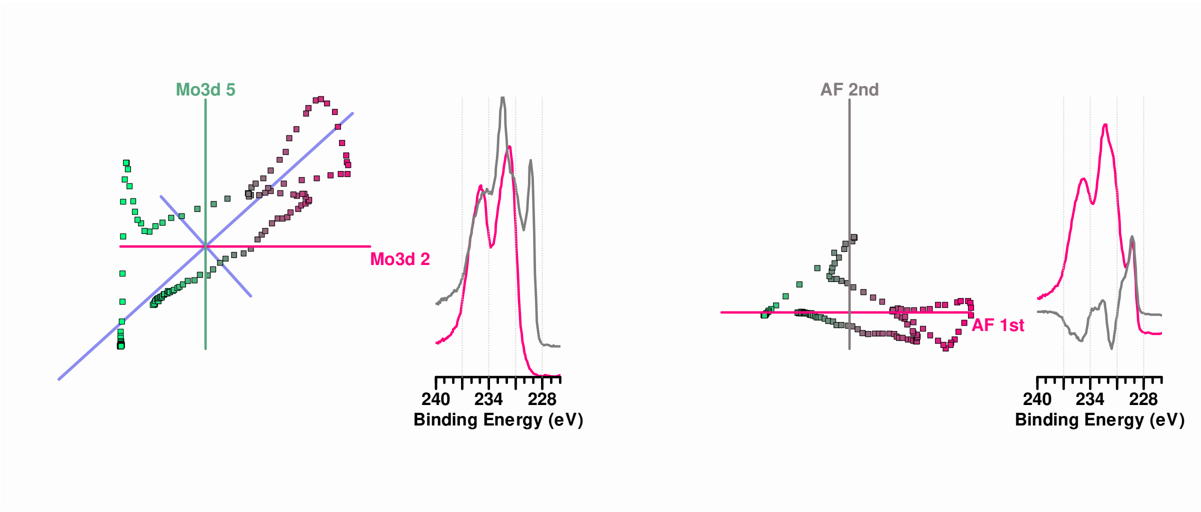

(a)

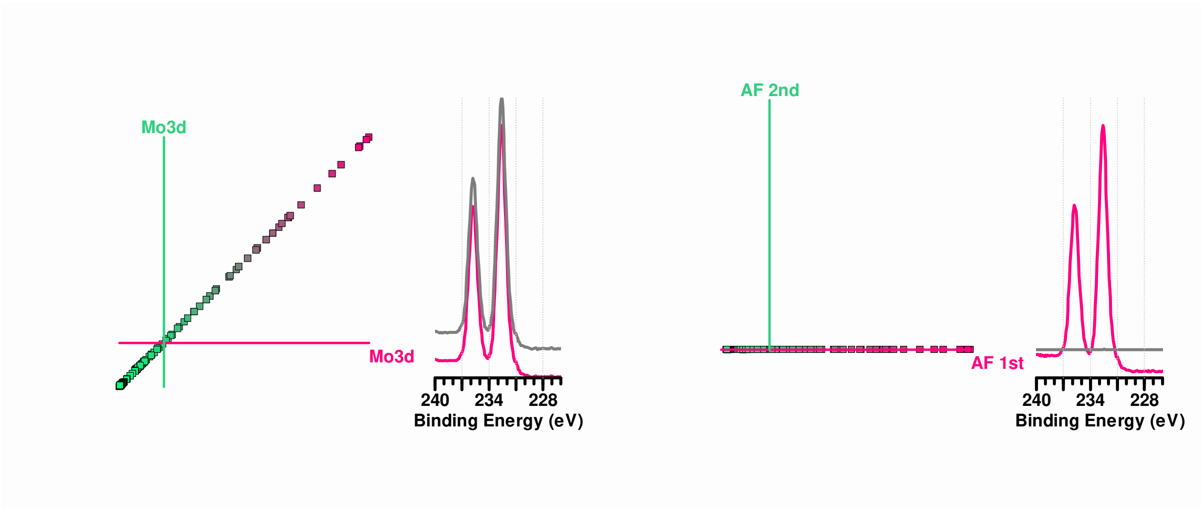

(b)

Figure 2. a) Comparison of scatter plots based on the spectra shown in Figure 1a that are distinct and PCA AFs calculated from these distinct spectra. b) Comparison of scatter plots based on identical spectra and PCA AFs calculated from these identical spectra. Note that the shape for the distribution of scatter points is unaltered between plotting scatter points formed from spectra or formed from PCA AFs.

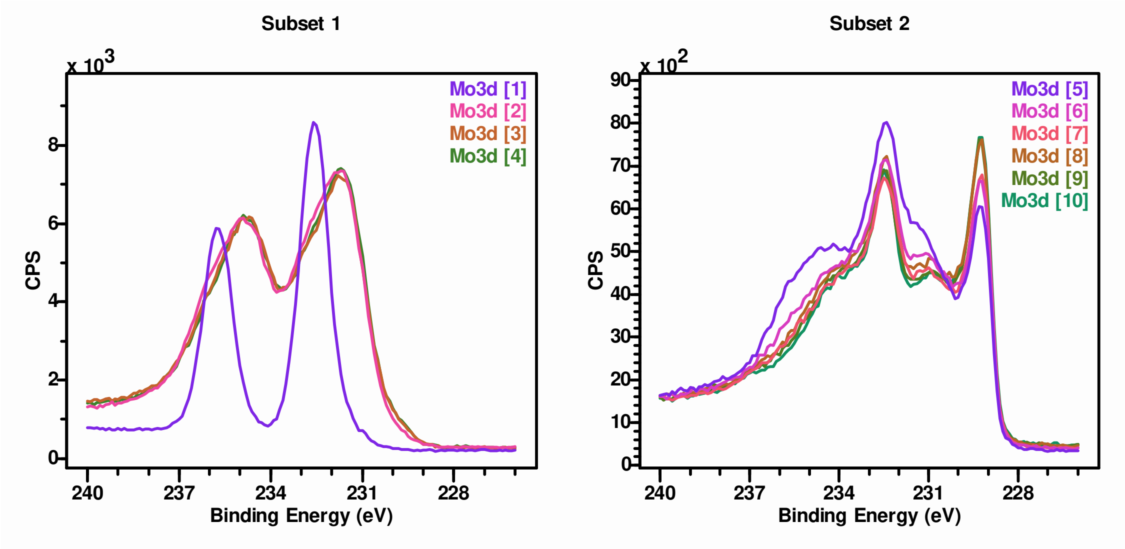

(a)

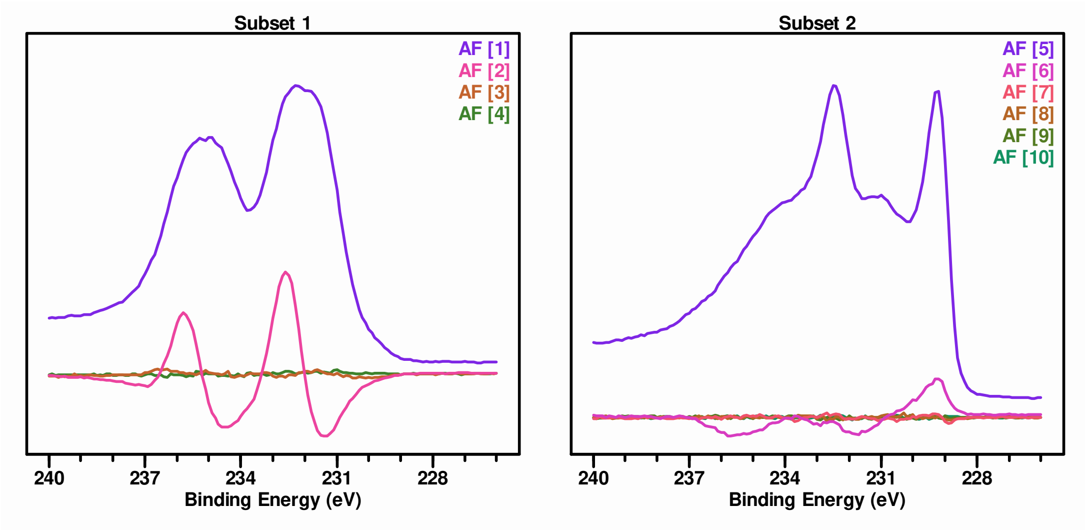

(b)

Figure 3. Classification of experimental data into two subsets of spectra for which each subset of spectra can be approximated by two PCA AFs and therefore interpreted as vectors belonging to two distinct planes in a n-dimensional vector space. These PCA classifications are consistent with spectra belonging to two distinct sample conditions induced by heating to 673 K and 723 K.

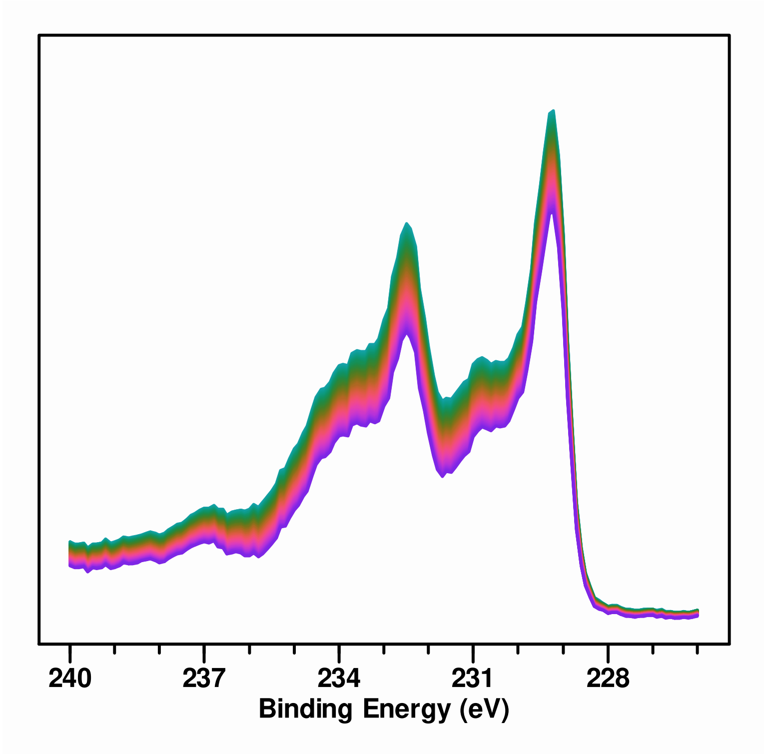

Figure 4. Examples of difference spectra calculated from subsampled spectra identified as belonging to a two-dimensional subspace of the MoO_3 film heated to 723 K.

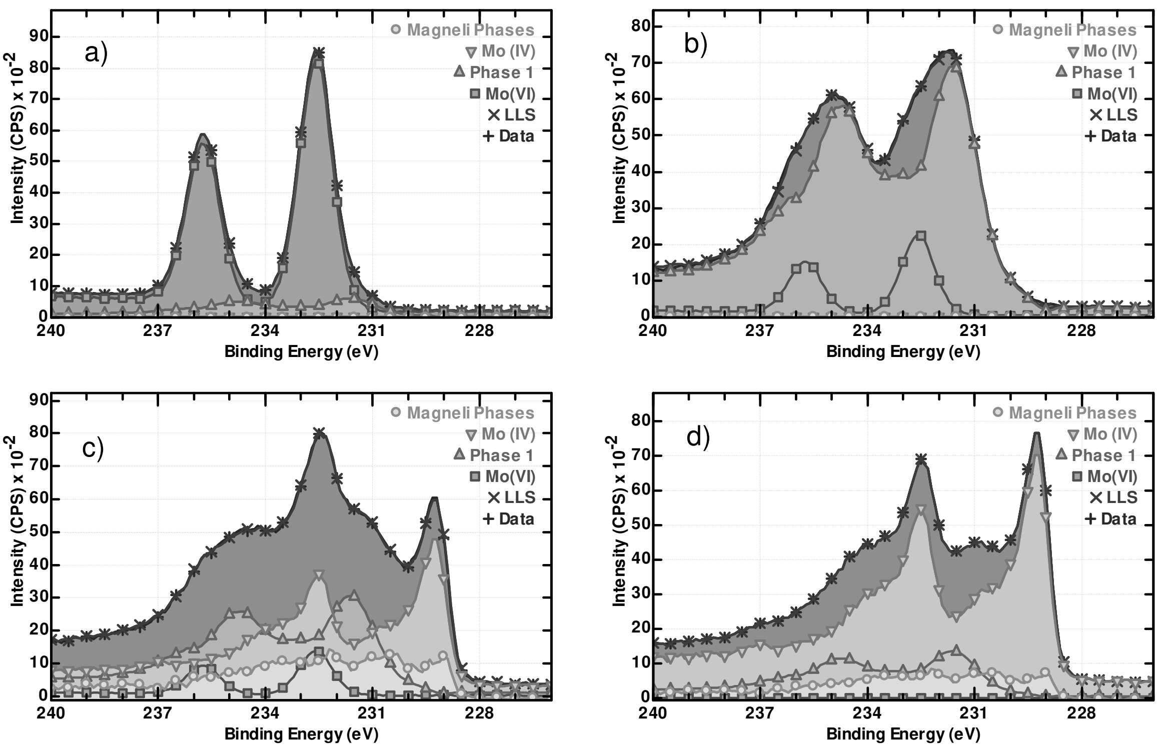

Figure 5. (a) Initial measurement of Mo (VI) oxide before raising the temperature of the sample. The fit shown in (a) is predominantly Mo (VI), however, a small proportion of signal indicated as Phase 1 Mo oxide can be detected. (b) Mo (VI) oxide after heating to 673 K. (c) Mo (VI) oxide once heated to 723 K. Note that both spectral components used in (b) are still necessary to fitting the spectrum in (c), but now additional components are required to achieve good data reproduction. (d) The final form of the sample following extended exposure at 723 K. The optimization solution in (d) suggests Mo (VI) oxide component is not required to fit these data. However, three components are required, which include the component labeled Phase 1. The evolution in spectra shown in Figure 1a is quantified in terms of these four component spectra in Figure 3.

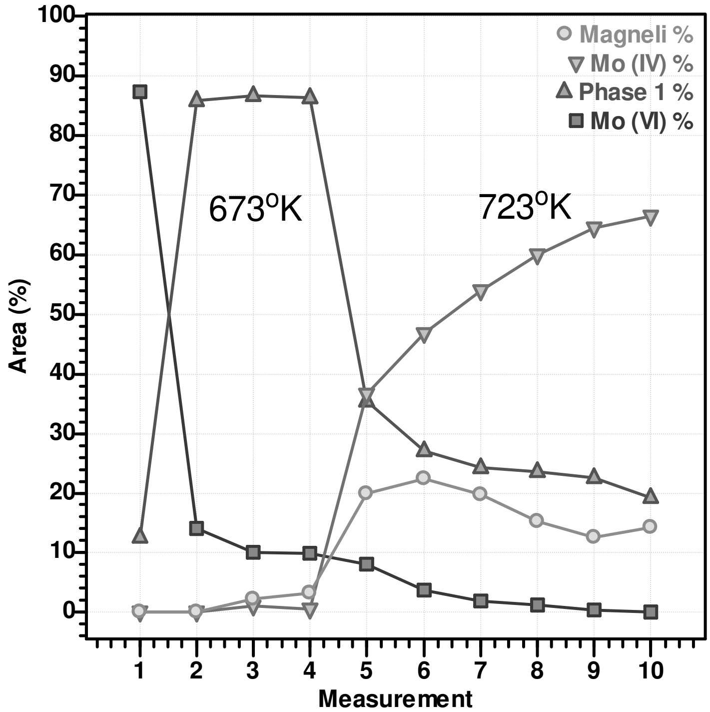

Figure 6. Profile of Mo 3d intensity calculated for each component spectrum illustrated in Figure 5. Spectra represent the response of the sample to specific temperatures, therefore %Area is plotted against the measurement index as indicated in Figure 1a where these indices are not only correlated with the temperature requested but also the duration over which the sample is exposed to these temperatures. The sample is initially measured at room temperature, then three measurements are performed following an increase in temperature to below or equal to 673 K, then six measures with temperature below or equal to 723 K.

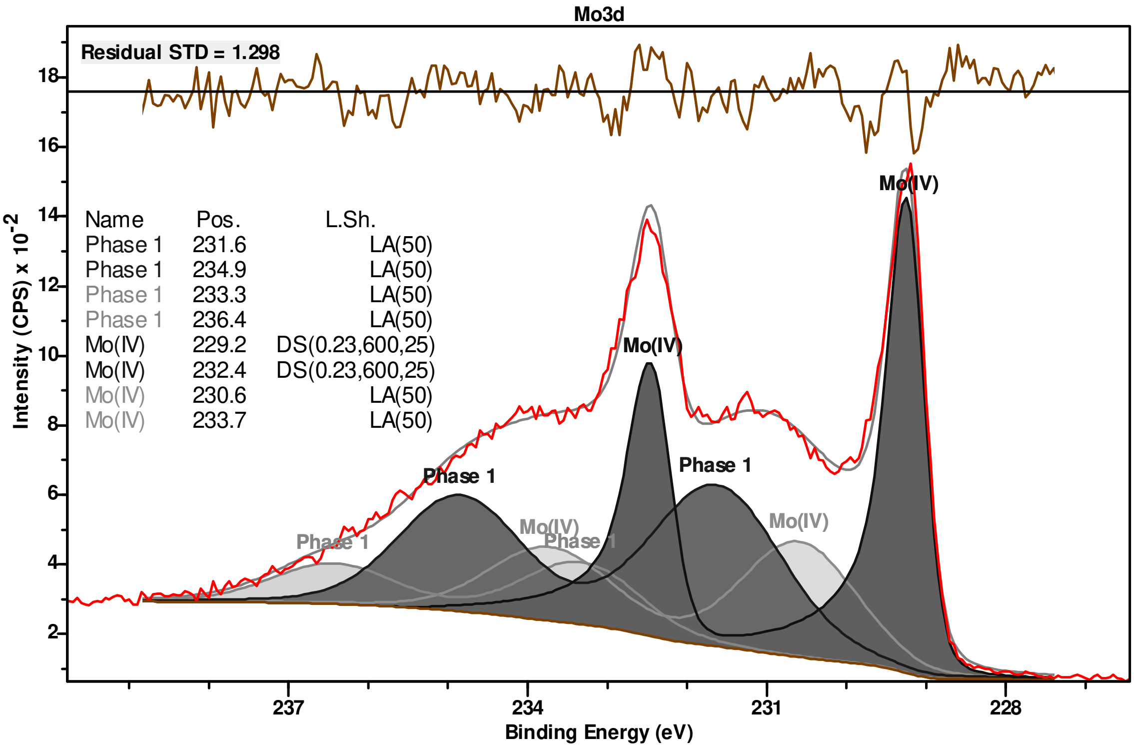

Figure 7. Mo (IV) oxide peak model based on mathematically defined line shapes. Note that the peak model mimics the fit shown in Figure 5d with the exception that these synthetic components to the peak model must also compensate for the absence of the signal indicated in Figure 5d as Magnéli oxide phases of molybdenum.

References

[1] I.A. de Castro, R.S. Datta, J.Z. Ou, A. Castellanos-Gomez, S. Sriram, T. Daeneke, K. Kalantar-zadeh, Molybdenum Oxides – From Fundamentals to Functionality, Advanced Materials. 29 (2017) 1701619. https://doi.org/10.1002/adma.201701619.

[2] L. Mai, F. Yang, Y. Zhao, X. Xu, L. Xu, B. Hu, Y. Luo, H. Liu, Molybdenum oxide nanowires: synthesis & properties, Materials Today. 14 (2011) 346–353. https://doi.org/10.1016/S1369-7021(11)70165-1.

[3] Y. Shi, B. Guo, S.A. Corr, Q. Shi, Y.-S. Hu, K.R. Heier, L. Chen, R. Seshadri, G.D. Stucky, Ordered Mesoporous Metallic MoO 2 Materials with Highly Reversible Lithium Storage Capacity, Nano Letters. 9 (2009) 4215–4220. https://doi.org/10.1021/nl902423a.

[4] J. Baltrusaitis, B. Mendoza-Sanchez, V. Fernandez, R. Veenstra, N. Dukstiene, A. Roberts, N. Fairley, Generalized molybdenum oxide surface chemical state XPS determination via informed amorphous sample model, Applied Surface Science. 326 (2015) 151–161. https://doi.org/10.1016/j.apsusc.2014.11.077.

[5] X. Liao, A.R. Jeong, R.G. Wilks, S. Wiesner, M. Rusu, M. Bär, X-ray irradiation induced effects on the chemical and electronic properties of MoO 3 thin films, Journal of Electron Spectroscopy and Related Phenomena. 212 (2016) 50–55. https://doi.org/10.1016/j.elspec.2016.08.004.

[6] A. Magnéli, G. Andersson, B. Blomberg, L. Kihlborg, Identification of Molybdenum and Tungsten Oxides by X-Ray Powder Patterns, Analytical Chemistry. 24 (1952) 1998–2000. https://doi.org/10.1021/ac60072a039.

[7] R.L. Smith, G.S. Rohrer, The Morphological Evolution of the MoO3(010) Surface during Reactions in Methanol–Air Mixtures, Journal of Catalysis. 180 (1998) 270–278. https://doi.org/10.1006/jcat.1998.2280.

[8] W. Gruenert, A.Yu. Stakheev, R. Feldhaus, K. Anders, E.S. Shpiro, Kh.M. Minachev, Analysis of molybdenum(3d) XPS spectra of supported molybdenum catalysts: an alternative approach, The Journal of Physical Chemistry. 95 (1991) 1323–1328. https://doi.org/10.1021/j100156a054.

[9] J.-G. Choi, L.T. Thompson, XPS study of as-prepared and reduced molybdenum oxides, Applied Surface Science. 93 (1996) 143–149. https://doi.org/10.1016/0169-4332(95)00317-7.

[10] P.A. Spevack, N.S. McIntyre, A Raman and XPS investigation of supported molybdenum oxide thin films. 1. Calcination and reduction studies, The Journal of Physical Chemistry. 97 (1993) 11020–11030. https://doi.org/10.1021/j100144a020.

[11] P.A. Spevack, N.S. McIntyre, Thermal reduction of molybdenum trioxide, The Journal of Physical Chemistry. 96 (1992) 9029–9035. https://doi.org/10.1021/j100201a062.

[12] A. Bertuch, G. Sundaram, M. Saly, D. Moser, R. Kanjolia, Atomic layer deposition of molybdenum oxide using bis(tert-butylimido)bis(dimethylamido) molybdenum, Journal of Vacuum Science & Technology A: Vacuum, Surfaces, and Films. 32 (2014) 01A119. https://doi.org/10.1116/1.4843595.

[13] B.E. Davis, N.C. Strandwitz, Aluminum Oxide Passivating Tunneling Interlayers for Molybdenum Oxide Hole-Selective Contacts, IEEE Journal of Photovoltaics. 10 (2020) 722–728. https://doi.org/10.1109/JPHOTOV.2020.2973447.

[14] N. Fairley, V. Fernandez, M. Richard-Plouet, C. Guillot-Deudon, J. Walton, E. Smith, D. Flahaut, M. Greiner, M. Biesinger, S. Tougaard, D. Morgan, J. Baltrusaitis, Systematic and collaborative approach to problem solving using X-ray photoelectron spectroscopy, Applied Surface Science Advances. 5 (2021) 100112. https://doi.org/10.1016/j.apsadv.2021.100112.

[15] V. Fernandez, N. Fairley, J. Baltrusaitis, Unraveling spectral shapes of adventitious carbon on gold using a time-resolved high-resolution X-ray photoelectron spectroscopy and principal component analysis, Applied Surface Science. 538 (2021) 148031. https://doi.org/10.1016/j.apsusc.2020.148031.

[16] P. Bargiela, V. Fernandez, C. Cardinaud, J. Walton, M. Greiner, D. Morgan, N. Fairley, J. Baltrusaitis, Towards a reliable assessment of charging effects during surface analysis: Accurate spectral shapes of ZrO2 and Pd/ZrO2 via X-ray Photoelectron Spectroscopy, Applied Surface Science. 566 (2021) 150728. https://doi.org/10.1016/j.apsusc.2021.150728.

[17] P.A. Spevack, N.S. McIntyre, A Raman and XPS investigation of supported molybdenum oxide thin films. 2. Reactions with hydrogen sulfide, The Journal of Physical Chemistry. 97 (1993) 11031–11036. https://doi.org/10.1021/j100144a021.

[18] D.O. Scanlon, G.W. Watson, D.J. Payne, G.R. Atkinson, R.G. Egdell, D.S.L. Law, Theoretical and Experimental Study of the Electronic Structures of MoO 3 and MoO 2, The Journal of Physical Chemistry C. 114 (2010) 4636–4645. https://doi.org/10.1021/jp9093172.

[19] Y.-J. Lee, T. Lee, A. Soon, Phase Stability Diagrams of Group 6 Magnéli Oxides and Their Implications for Photon-Assisted Applications, Chemistry of Materials. 31 (2019) 4282–4290. https://doi.org/10.1021/acs.chemmater.9b01430.

[20] B. Moeini, M.R. Linford, N. Fairley, A. Barlow, P. Cumpson, D. Morgan, V. Fernandez, J. Baltrusaitis, Definition of a new (Doniach-Sunjic-Shirley) peak shape for fitting asymmetric signals applied to reduced graphene oxide/graphene oxide XPS spectra, Surface and Interface Analysis. (2021). https://doi.org/10.1002/sia.7021.

[21] G.H. Major, V. Fernandez, N. Fairley, M.R. Linford, A detailed view of the Gaussian–Lorentzian sum and product functions and their comparison with the Voigt function, Surface and Interface Analysis. 54 (2022) 262–269. https://doi.org/10.1002/sia.7050.

[22] E. Bêche, P. Charvin, D. Perarnau, S. Abanades, G. Flamant, Ce 3d XPS investigation of cerium oxides and mixed cerium oxide (CexTiyOz), Surface and Interface Analysis. 40 (2008) 264–267. https://doi.org/10.1002/sia.2686.

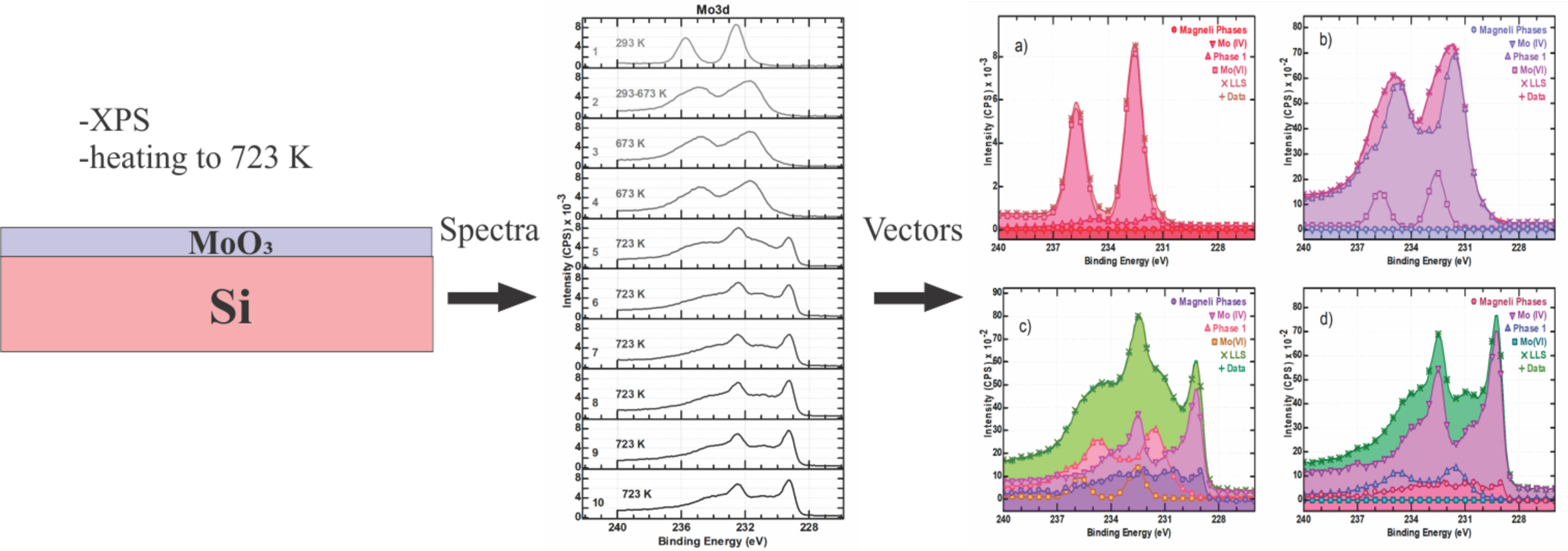
-XPS
-heating to 723 K
MoO3
Si
Spectra
Vectors
Mo3d
293 K
293-673 K
673 K
673 K
723 K
723 K
723 K
723 K
723 K
723 K
Intensity (CPS) x 10-3
Binding Energy (eV)
a)
b)
c)
d)
Magneli Phases
Mo (IV)
Phase 1
Mo(VI)
LLS
Data
Intensity (CPS) x 10-2